Comparing the Excited State Dynamics of CH_2OO, the Simplest Criegee Intermediate, Following Vertical *versus* Adiabatic Excitation.

Ernest Antwi,[1] Jordyn M. Ratliff,[1] Michael N. R. Ashfold[2] and Tolga N. V. Karsili[1,*]

[1]*Department of Chemistry, University of Louisiana at Lafayette, Lafayette, LA 70503, USA*

[2]*School of Chemistry, University of Bristol, Cantock's Close, Bristol, BS8 1TS, UK*

*Author to whom correspondence should be addressed: tolga.karsili@louisiana.edu

Abstract

Ab initio molecular dynamics studies of CH_2OO molecules following excitation to the minimum energy geometry of the strongly absorbing S_2 ($^1\pi\pi^*$) state reveal a much richer range of behaviors than just the prompt O–O bond fission, with unity quantum yield and retention of overall planarity, identified in previous vertical excitation studies from the ground (S_0) state. Trajectories propagated for 100 fs from the minimum energy region of the S_2 state show a high surface hopping (non-adiabatic coupling) probability between the near-degenerate S_2 and S_1 ($^1n\pi^*$) states at geometries close to the S_2 minimum, that enables population transfer to the optically dark S_1 state. >80% of the excited population undergoes O–O bond fission on the S_2 or S_1 potential energy surfaces (PESs) within the analysis period, mostly from non-planar geometries wherein the CH_2 moiety is twisted relative to the COO plane. Trajectory analysis also reveals recurrences in the O–O stretch coordinate, consistent with the resonance structure observed at the red end of the parent S_2–S_0 absorption spectrum and a small propensity for out-of-plane motion after non-adiabatic coupling to the S_1 PES that enables access to a conical intersection between the S_1 and S_0 states and cyclization to dioxirane products.

Introduction

Criegee intermediates (CIs) are carbonyl oxides that play vital roles in Earth's troposphere, where they are formed via a [3+2]-cycloaddition reaction involving volatile alkenes and ozone.[1–8] CIs are implicated in enhancing the oxidizing capacity of the troposphere and in the formation of less volatile species that may condense to form secondary organic aerosols (SOAs).[6–14]

The exoergicity of alkene ozonolysis reactions ensures that the nascent CIs are formed highly internally excited and may undergo unimolecular decay or lose vibrational energy via collisions with surrounding gas molecules. The stabilized CIs (sCIs) formed by the latter process may also undergo (generally much slower) unimolecular decay or participate in bimolecular reactions with trace atmospheric gases.[15–25]

As with carbonyl compounds, CIs possess π-orbitals which manifest in strongly absorbing $\pi^* \leftarrow \pi$ transitions, resulting in population of $\pi\pi^*$ excited states.[18,23,24,26–30] The π-conjugation extends over the COO moiety, which leads to a bathochromic shift of the $\pi^* \leftarrow \pi$ absorption profile *cf.* that of the corresponding carbonyl compound.[31–34] These $\pi^* \leftarrow \pi$ absorptions have been used to probe the bimolecular chemistry of CIs and, particularly in the case of larger and more functionalized CIs such as methyl vinyl ketone oxide and methacrolein oxide, may contribute to their removal by solar photolysis.[35–37]

Formaldehyde oxide, CH_2OO, is the simplest Criegee intermediate. It is formed in the ozonolysis of alkenes such as isoprene,[38] the second most abundant volatile organic compound after methane.[39] The UV absorption spectroscopy and photochemistry of CH_2OO have been the focus of many experimental[15,16,18–22,30] and computational[17,23–25,40,41] studies. Its strongly absorbing $^1\pi\pi^*$ state (the S_2 state) covers the 420-280 nm range – with a peak absorption cross-section of 1.2×10^{-17} cm^2 at a wavelength λ ~340 nm.[18] Excitation within this band results in O–O bond

fission, yielding $O(^1D)$ and $O(^3P)$ atoms together with CH_2O (formaldehyde) products. The CH_2O molecules accompanying the majority $O(^1D)$ products are formed with high internal energies.[26,30] Recently, we reported trajectory surface hopping (TSH) simulations that modelled the excited state dynamics of CH_2OO starting from a Wigner distribution based on the ground (S_0) state equilibrium geometry.[28,42] Trajectories initiated by vertical excitation to the S_2 state were found to yield $O + CH_2O$ products in times t <50 fs, with unity quantum yield. Such trajectory simulations mimic photochemical experiments conducted by exciting at the absorption band maximum under jet-cooled conditions. Since these dynamics occur promptly, initiating trajectories in this way cannot capture dynamics that occur when exciting at the long wavelength edge of the $S_2 \leftarrow S_0$ absorption band, where the observed vibronic resonances clearly imply some longer-lived population in the S_2 state.[18,22] Further, our previous simulations of the electronic absorption spectrum of CH_2OO using a Wigner distribution based on the ground state minimum energy geometry and vertical excitations obtained using complete active space second order perturbation (CASPT2) theory successfully reproduced the shorter wavelength and peak absorption regions of the experimental $S_2 - S_0$ spectrum but failed to capture the observed long wavelength tail.[42] This, again, implies that the S_2 state geometry is sufficiently distorted from that of the ground state that simulations using initial geometries (and associated momenta) from a Wigner distribution based on the S_0 minimum energy geometry are not sufficient to capture the behavior of population excited to the region of the S_2 minimum.

The present work investigates the excited state dynamics of CH_2OO using CASPT2 surface hopping methods and initiating trajectories at regions close to the minimum of the $S_2(^1\pi\pi^*)$ state rather than in the vertical region, to better understand the dynamics following electronic excitation at the long wavelength edge of the CH_2OO absorption spectrum. The former and

current studies are henceforth identified as 'vertical' and 'adiabatic' (as in vibrationally adiabatic) excitations, respectively. The adiabatic calculations offer new insights into the non-adiabatic coupling mechanism by which population near the S_2 potential minimum transfers to the (optically dark) S_1 potential energy surface (PES), reveal recurrences in the O–O stretch motion on both the S_2 and S_1 PESs and show how subsequent out-of-plane motions can access a (previously reported) conical intersection (CoIn) between the S_1 and S_0 PESs and enable cyclization to dioxirane.[43] Most adiabatically excited molecules still dissociate by O–O bond fission, however, but – in contrast to the situation following vertical excitation to the S_2 state – with loss of overall planarity. Two contributory causes for the observed dominance of non-planar dissociations from both the S_2 and S_1 excited states following adiabatic preparation of $CH_2OO(S_2)$ molecules are identified.

Computational Methodology

Using Gaussian 16,[44] the minimum energy geometry and associated normal mode wavenumbers of the S_2 state were obtained at the B3LYP/6-311++G** level of theory, a level of theory that has previously been judged to perform well for CH_2OO.[17,45] The resulting optimized geometry and normal modes were used to generate the initial positions and momenta of the trajectories which were randomly sampled from a S_2 state Wigner distribution of uncoupled harmonic oscillators that accounts for the zero point energy in the sampling of the quantum vibrational levels. TSH simulations were performed using Newton-X.[46,47] Nuclear coordinates were propagated by integrating Newton's equations using the velocity Verlet method, while the electronic coordinates were propagated by numerically solving the time-dependent Schrödinger equation using Butcher's fifth-order Runge-Kutta method in steps of 0.025 fs.[48] Trajectories

were initiated on the S_2 state and the energies and gradients of the seven lowest singlet states were calculated "on-the-fly" using the single-state, single-reference variant of multistate CASPT2 (SS-SR-CASPT2) in conjunction with the cc-pVDZ basis set.[49] As before,[50] the SS-SR-CASPT2 calculations were based on a state-averaged complete active space self-consistent field (CASSCF) reference wavefunction and an active space comprising 10 electrons in 8 orbitals (depicted in Fig. S1 of the supporting information). These were performed via the BAGEL interface to Newton-X.[51] The state hopping probabilities were evaluated by calculating the non-adiabatic coupling matrix elements from the SS-SR-CASPT2 computations. 80 trajectories were propagated out to a maximum time t = 100 fs, with a step size of 0.5 fs. Note, the S_2 minimum energy geometry (S_2^{min}) and normal modes were generated at a different level of theory to that used to determine the energies and gradients for the TSH simulations. This allowed sampling of a greater fraction of the S_2 minimum and the surrounding configuration space and allowed a better description of the dynamics following excitation to the long wavelength end of the electronic absorption spectrum of CH_2OO.

Additional PE profiles and stationary points were computed at the CASPT2/aug-cc-pVTZ level of theory using the same active space and the Molpro computational package [52,53] to refine the energetics associated with the various motions revealed by the TSH simulations.

The equilibrium values for the O–O bond distance and ∠COO bond angle in the S_2 state returned by these CASPT2 calculations (1.613 Å and 98.9°, respectively) agree with those found in previous MRCI/cc-pVTZ calculations [ref 17] and are reassuringly similar to those provided by the present (and previous [ref Lee et al]) B3LYP/6-311++G** calculations (1.623 Å and 90.5°).

Results and Discussion

The ground state minimum energy geometry (S_0^{min}) of CH_2OO, given in Fig. 1(a), has all atoms in a common plane. The C–O and O–O bond lengths (R_{CO} and R_{OO}) and the COO bond angle ($\angle$COO) determined at the B3LYP/6-311++G** level of theory are, respectively, 1.27 Å, 1.33 Å and 119.37° – consistent with previous experimental and theoretical values.[54] As Fig. 2 shows, the first excited singlet state is the optically 'dark' S_1 state, arising via an $\pi^*\leftarrow$n transition. The lowest excited singlet state of CH_2OO with appreciable oscillator strength following vertical excitation from S_0 is the S_2 state. This arises via a $\pi^*\leftarrow\pi$ electron promotion in which the participating orbitals have good spatial overlap (as shown in Fig. 2(b)) and is responsible for the strong absorption that peaks at a wavelength λ ~340 nm in the experimentally measured spectrum.[55] Figure 2(a) shows that the diabatic S_2 potential correlates to $O(^3P)$ + $^3CH_2O$ products but also highlights that the S_2 (and S_1) potentials are involved in complex four-state CoIns with the S_3 and S_4 potentials (CoIn1) and with the S_5 and S_6 potentials (CoIn2) at planar geometries, the first of which facilitates non-adiabatic coupling from the S_2 state to the $O(^1D)$ + $CH_2O(S_0)$ limit.

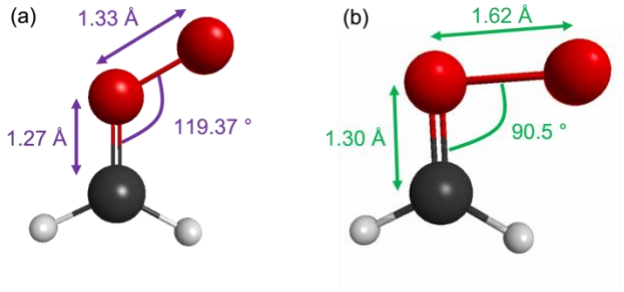

Figure 1: Minimum energy geometries of the (a) ground state and (b) second (S_2) excited electronic states of CH_2OO derived using the DFT level of theory.

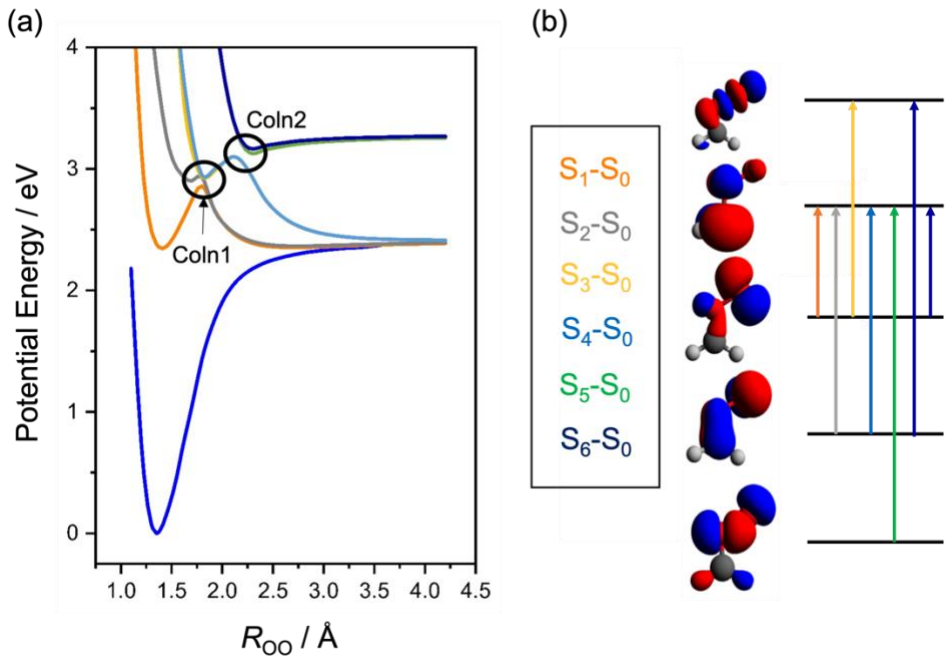

Figure 2: (a) Adiabatic PE profiles along the R_{OO} coordinate of CH_2OO for the lowest six singlet electronic states constrained to planar geometries. (b) Orbitals and dominant orbital promotions associated with excitations to the lowest six singlet excited states, color coded so as to match with the excited state PECs shown in panel (a). The S_6-S_0 transition involves a double-excitation as depicted by the two orbital promotions in dark blue. Reproduced from Esposito *et al*., *Photochem. Photobiol.* **2021**, *98*, 763–772. Copyright 2021 Wiley.

The S_2^{min} geometry of CH_2OO determined in the present study is also planar but, as Fig. 1(b) shows, ∠COO is reduced to 90.5° and R_{CO} and R_{OO} have both increased (to 1.30 Å and 1.62 Å, respectively). These bond extensions and the change in bond angle can be understood by recognizing the reduction in bond order and change in hybridization at the central O atom that accompanies π*←π excitation.

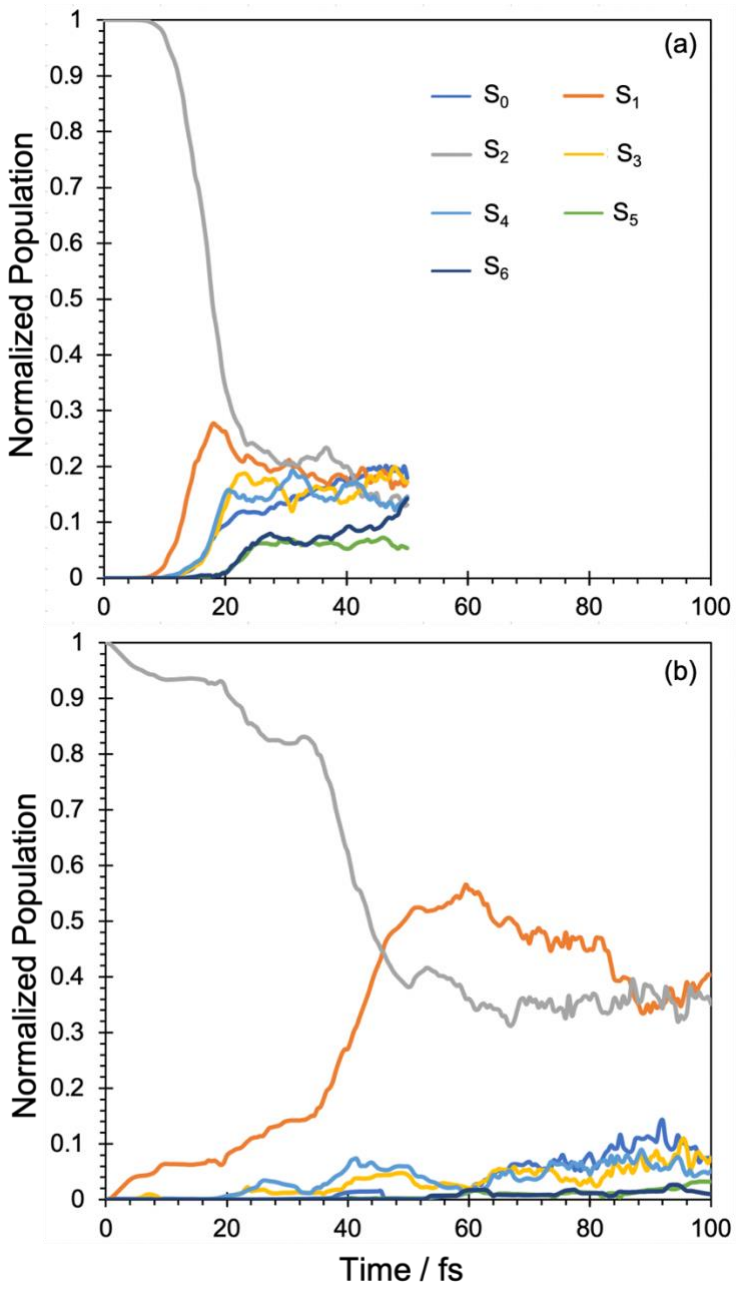

Figure 3: Normalized state populations from trajectories propagated as a function of time following (a) vertical and (b) adiabatic excitation to the S_2 state at time $t = 0$. The respective state populations are color coded to match the potentials shown in Figure 2, as shown in the inset in panel (a).

Figs. 3(a) and 3(b) show, respectively, the time evolving populations of the seven lowest singlet states of CH_2OO following vertical and adiabatic excitation of the S_2 state. The data underpinning Fig. 3(a) are from previous work,[50] while the data shown in Fig. 3(b) is entirely new. As Fig. 3(a) shows, the S_2 state population prepared by vertical excitation decays rapidly, to ~20% of its starting value within *ca*. 20 fs – with population transferring to the S_0, S_1, S_3, S_4, S_5 and S_6 states. The trajectories plotted in Fig. 4(a) clearly show that the dominant decay path following photoexcitation is O–O bond fission and formation of $O(^1D)$ + CH_2O products. The departing O atom recoils in the plane defined by the CH_2OO molecule. Such findings are entirely consistent with previous experimental measurements conducted around the peak of the S_2–S_0 absorption of CH_2OO.[30,56]

The present calculations predict much richer behavior following adiabatic promotion to S_2^{min}. As Fig. 3(b) shows, the S_2 state population at t = 20 fs following adiabatic excitation is still at ~90% of the starting value. This surviving fraction has fallen to ~50% by t = 50 fs and to ~35% by t = 100 fs, and most of the transferred population couples to the S_1 state. Trajectories initiated by adiabatic promotion should provide a better probe of experimental measurements made at the long wavelength end of the S_2–S_0 absorption spectrum. Fig. 4(b), which has been color coded to illustrate when each trajectory transfers to other states, clearly shows that not all trajectories have undergone irreversible O–O bond elongation within the 100 fs propagation window. This, and the larger remaining S_2 population, both align with the parent vibronic resonances observed in the long wavelength tail of the S_2–S_0 spectrum.[24,30,56]

Another noteworthy observation from Fig. 4(b) are the trajectories showing oscillatory motion within the 100 fs propagation time window. These oscillations occur within the range R_{OO} ~1.5-1.8 Å for trajectories that remain on the S_2 PES (R_{OO} ~1.3-1.6 Å for trajectories that have jumped

to the S_1 PES), *i.e.* these trajectories remain as parent CH_2OO molecules that are trapped in the S_2 (or S_1) potential wells. The periods of oscillation associated with these trajectories are in the range 40-90 fs. The average period of ~50 fs equates to a wavenumber of ~650 cm^{-1}, similar to the peak spacing (~690 cm^{-1}) in the long wavelength tail of the room temperature absorption spectrum of CH_2OO.[18,22] This serves to reinforce previous theoretical accounts that the excited state O–O stretch motion is a dominant contributor to this vibronic structure.[24]

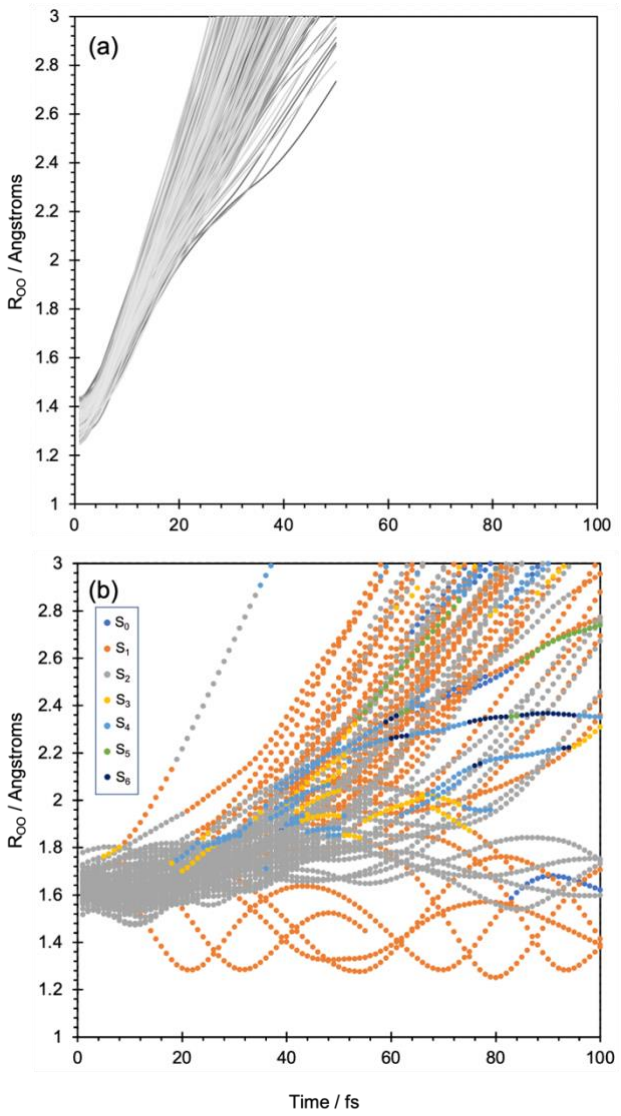

Figure 4: R_{OO} values of the (a) vertically and (b) adiabatically propagated trajectories as a function of time. The time at which any given trajectory 'hops' from one PES to another in panel (b) is shown by the appropriate color change.

We now look more closely at the evolving population following adiabatic excitation to the S_2 state. Analysis of the trajectories reveals three broad classes of photochemical outcome at the end of the trajectory classified, in order of decreasing probability, as: (1) dissociation to form O + CH_2O products; (2) surviving as a parent CH_2OO molecule throughout the analysis period; and (3) cyclization to form dioxirane. The pie-charts in Fig. 5 show the percentage of trajectories exhibiting each of these classes of behavior following (a) vertical and (b) adiabatic excitation to the S_2 state. As Fig. 5(a) shows, all vertically excited trajectories undergo O–O bond fission within t = 50 fs. Further analysis of these trajectories shows minimal loss of planarity in all cases. Most (~82%) of the adiabatically prepared trajectories also result in O–O bond fission (within 100 fs) but, as Fig. 4(b) shows, the majority of these dissociations are predicted to occur after non-adiabatic coupling to the S_1 state and, as Fig. 5(c) shows, most occur from non-planar geometries; the velocity vector of the departing O atom is out of the plane defined by the parent CH_2O partner. (The parent motion leading to this outcome can be viewed as a torsion of the CH_2 group about the C_2 rotation axis of the surviving H_2CO moiety (as described above) or of the terminal O about this same axis). Henceforth, we characterize the angle between the planes defined by the CH_2 group and the COO moiety as ϕ; $\phi = 0$ in the $CH_2OO(S_0)$ parent. ~15% of the adiabatically excited trajectories remain as intact CH_2OO molecules throughout the 100 fs analysis period (but would likely dissociate if followed to yet longer times), while ~3% cyclize to form ground state dioxirane products within 100 fs.

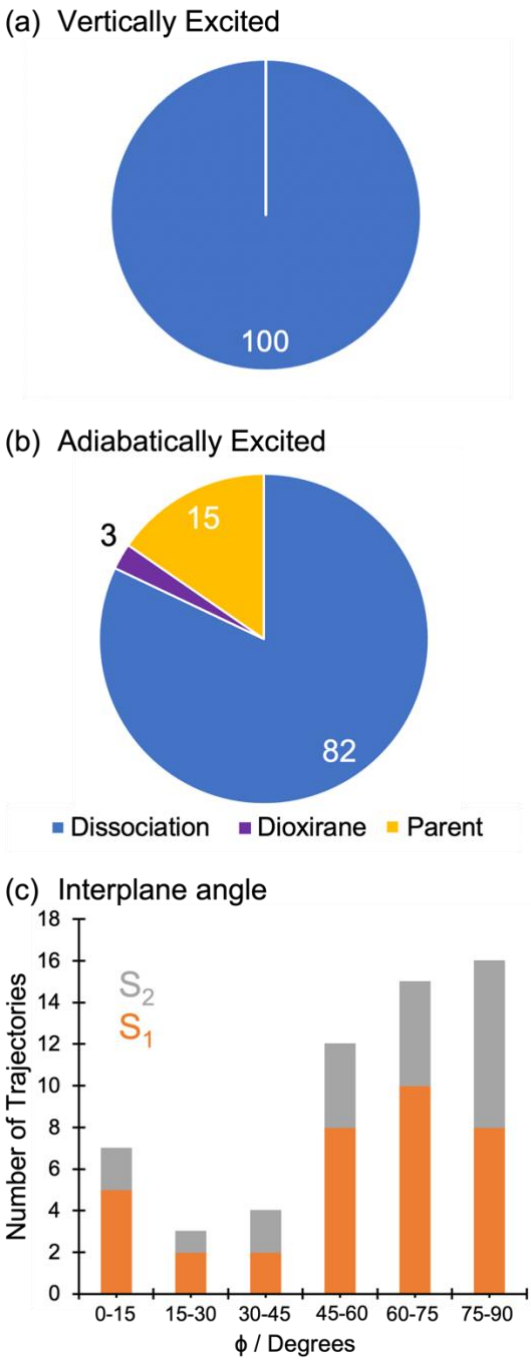

Figure 5: Pie charts showing the fractions of trajectories that result in (i) O–O bond dissociation, (ii) remain as CH_2OO (parent), or (iii) form dioxirane, derived from analysis of trajectories following (a) vertical excitation to the S_2 state, analyzed out to t = 50 fs and (b) adiabatic excitation to the S_2 state analyzed out to t = 100 fs. The bar chart (c) shows the numbers of dissociating trajectories following adiabatic excitation sub-divided by the excited state on which dissociation occurs (analyzed once $R_{OO} \geq 2$ Å) and by ϕ (binned into 15° intervals).

The fraction of each outcome will be sensitive to the initial Wigner sampling, but the realization that most dissociations occur from non-planar geometries, that some excited CH_2OO species survive for several vibrational periods and the predicted minor channel to dioxirane products following adiabatic excitation to the S_2 state are all noteworthy – and different from that observed following vertical excitation to the S_2 state.

Dioxirane formation from photoexcited CH_2OO was predicted in previous CASSCF trajectory studies,[43] starting from the optically-dark S_1 state. ~30% of the initially excited S_1 population in that state was found to evolve towards a CoIn between the S_1 and S_0 states at an out-of-plane geometry that enabled internal conversion and ultimate dioxirane formation. It is not clear if such regions of configuration space are sampled following excitation to the S_2 state, however, as there is no equivalent S_2/S_1 CoIn along the relevant out-of-plane coordinates. The same study located the well-documented S_2/S_1 CoIn along the O–O stretch coordinate (CoIn1 in Fig. 2(a)) and hypothesized that this might promote the $S_2 \rightsquigarrow S_1$ internal conversion required to enable subsequent motion on the S_1 PES towards the out-of-plane S_1/S_0 CoIn. The present study casts doubt on such a mechanism, since it would require a substantial redistribution of the internal energy and a complete reversal of the nuclear momenta against the gradient of steepest descent (*i.e.* against O–O bond fission once in the region of CoIn1).

The present adiabatically excited trajectories offer much clearer insights into the motions responsible for internal conversion from S_2 to the S_1 (and S_0) states. Simply put, the trajectories show that $S_2 \rightsquigarrow S_1$ internal conversion in the vicinity of S_2^{min} is not driven at CoIn1; the S_2 and S_1 states are energetically sufficiently close at S_2^{min} that the adiabatically trapped S_2 population can couple to the S_1 state. Such coupling is revealed as surface hops in the present trajectory study, that occur at geometries with non-degenerate S_2/S_1 energies.

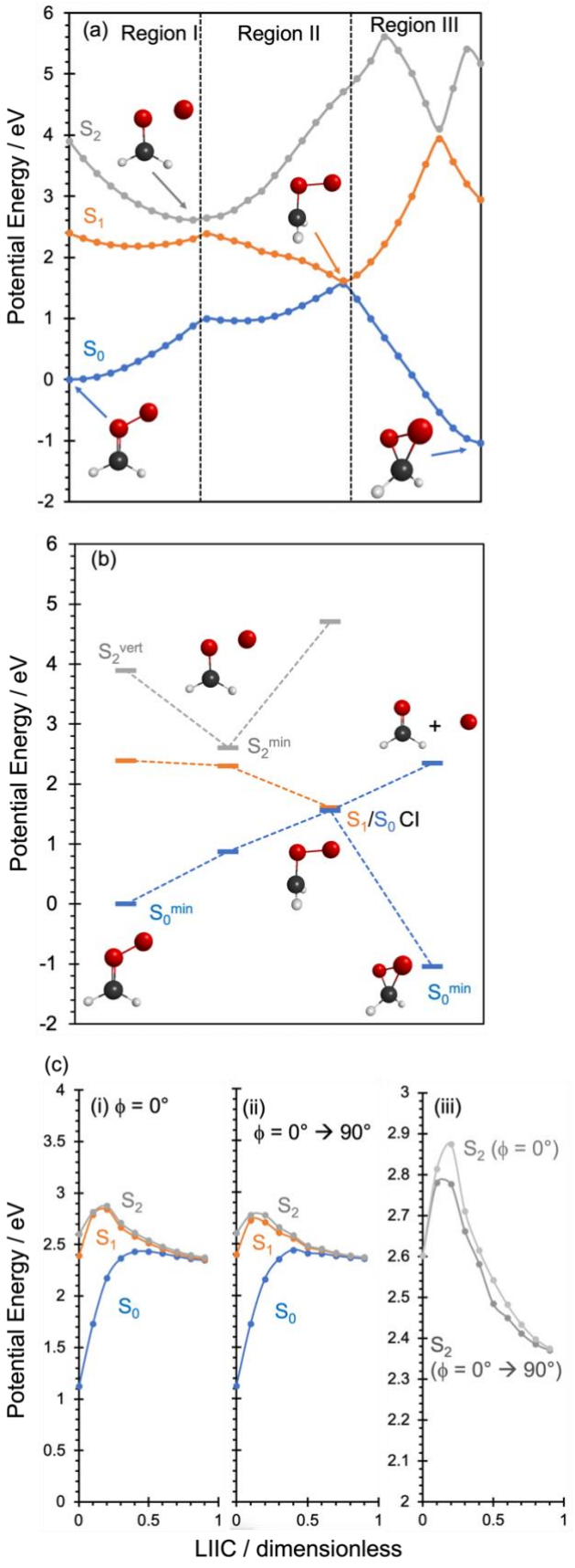
(a)
Region I
Region II
Region III
Potential Energy / eV
S2
S1
S0
(b)
S2vert
S2min
S1/S0 CI
S0min
S0min
+
(c)
(i) ϕ = 0°
(ii)
ϕ = 0° → 90°
(iii)
S2 (ϕ = 0°)
S2
(ϕ = 0° → 90°)
Potential Energy / eV
LIIC / dimensionless

Figure 6: (a) CASPT2/aug-cc-pVTZ calculated profiles associated with motion along LIICs between the vertical and minimum energy regions of the S_2 PES (Region I), between the S_2^{min} and the out-of-plane S_1/S_0 CoIn (Region II) and then between this CoIn and the dioxirane minimum energy geometry on the S_0 PES (Region III). (b) CASPT2/aug-cc-pVTZ calculated energies of key stationary points, including the asymptotic energy for forming $O(^1D) + CH_2O(S_0)$ products (calculated at $R_{OO} = 3.5$ Å). (c) CASPT2/aug-cc-pVTZ calculated profiles associated with motion along a LIIC between the S_2^{min} (right hand edge of Region I in panel (a)) and the $O(^1D) + CH_2O$ products at $R_{OO} = 3.5$ Å (upper right hand asymptote in panel (b)), assuming (i) that all atoms remain in a common plane (*i.e.* $\phi = 0°$) and (ii) that ϕ evolves smoothly from 0 to 90° along the LIIC. The energy profiles for the planar *vs*. progressively more non-planar dissociation paths are compared in (c, iii).

To explore this further, PE profiles have been computed at the CASPT2/aug-cc-pVTZ level by various linear interpolations in internal coordinates (LIICs). Fig. 6(a) shows calculated profiles connecting the S_2 vertical region to S_2^{min}, between the latter geometry and the out-of-plane S_1/S_0 CoIn and from this CoIn to the ground state of dioxirane. Region I displays the linearly interpolated reaction path between the minimum energy geometries of the S_0 and S_2 states and clearly reveals the near-degeneracy of the S_2 and S_1 states at the S_2^{min} geometry. Following $S_2 \dashrightarrow S_1$ internal conversion in the vicinity of S_2^{min}, an appropriate out-of-plane motion coupled with some O–O bond compression can lead to an S_1/S_0 CoIn (Region II). Subsequent evolution on the S_0 PES to form dioxirane following non-adiabatic coupling at this S_1/S_0 CoIn is predicted to be barrierless (Region III).

But the simulations reveal that only ~3% of the adiabatically excited S_2 trajectories lead to cyclization and dioxirane formation. Most result in O–O bond fission, and most of these dissociations occur from non-planar geometries. Both these findings can be understood from the CASPT2/aug-cc-pVTZ stationary points displayed in Fig. 6(b) and the potential energy profiles along LIICs describing dissociation from both planar and non-planar geometries shown in Fig. 6(c). As Fig. 6(b) shows, the energetic threshold for forming $O(^1D) + CH_2O(S_0)$ products lies below S_2^{min}. The profiles shown in Fig. 6(c) show that the S_2 and S_1 PESs converge in energy

towards and beyond CoIn1 and that the energy of the barriers to O–O bond fission are similar to the adiabatic excitation energy at S_2^{min}. The O–O separation will thus only increase rather slowly as the dissociating molecule passes through the region of CoIn1, allowing nuclear momenta orthogonal to this coordinate (*e.g.* out-of-plane motions) introduced in the initial Wigner sampling to influence the eventual recoil. Trajectory analysis shows this to be a major contributor to the preponderance of out-of-plane (*i.e.* $\phi > 0°$) dissociations from both the S_2 and (following internal conversion) the S_1 states.

The potentials shown in Fig. 6(c) identify a second factor encouraging non-planar dissociation. Panels (i) and (ii) present PE profiles starting from the S_2^{min} geometry along two closely related LIICs along the R_{OO} stretch coordinate. In the former, R_{OO} is stepped out to 3.5 Å with ϕ fixed at 0°. The latter LIIC involves the same extension of R_{OO}, but in tandem with a progressive increase in ϕ from 0° to 90°. As the comparison in (c, iii) shows, even an ~15° loss of planarity results in a discernible lowering of the S_2 (and S_1) barrier heights and thus encourages dissociation to the observed $O(^1D) + CH_2O(S_0)$ products.

Clearly it will be interesting to explore the analogous dynamics from the S_2^{min} geometries of CIs of greater molecular complexity, like methyl vinyl ketone oxide and methacrolein oxide (CIs formed in the ozonolysis of isoprene), with greater numbers of internal degrees of freedom (potential acceptor modes) that could facilitate energy flow out of the O–O stretch coordinate and potentially reduce the rate of dissociation and boost branching into the corresponding oxirane.

Conclusions

The present work presents CASPT2 TSH calculations that reveal the dynamics following adiabatic excitation to the strongly absorbing S_2 state of CH_2OO and compares the observed behavior with that found in the case of vertical excitation to the same excited state. Previous findings that a Wigner distribution based on the S_0 minimum energy geometry is inadequate for describing the photodynamics of CH_2OO following excitation across the entire S_2–S_0 absorption spectrum are confirmed.[29,50] The present work shows that the longer wavelength dynamics of interest can be successfully captured by Wigner sampling from initial positions and momenta generated from the optimized S_2 state minimum. Only a modest number of trajectories are propagated but, given that only two major channels are observed following adiabatic excitation to the S_2 state, the present simulations should be statistically sound within the level of theory used.

Vertical excitation to the S_2 state results in prompt O–O bond fission, with unity quantum yield; the fragment recoil velocity vector typically lies in the plane defined by the parent molecule. Adiabatic excitation to the S_2 state results in a much richer range of behaviors. The present TSH data reveal recurrences in the O–O stretch coordinate on the S_2 (and S_1) PESs, consistent with the resonance structure observed at the red end of the $CH_2OO(S_2–S_0)$ absorption spectrum. The trajectory data also offer new insights into the non-adiabatic coupling between the near-degenerate S_2 and S_1 states at geometries close to S_2^{min}, that enables population transfer to the optically dark S_1 PES. Out-of-plane distortions (not least those introduced by the initial Wigner sampling) are shown to be important. They reduce the barrier to dissociation on the S_2 and S_1 PESs in the region of CoIn1, thereby boosting the O–O bond fission probability. Out-of-plane motions following non-adiabatic coupling to the S_1 state also offer a route to a S_1/S_0 CoIn that

facilitates cyclization to dioxirane – a predicted minor (but non-zero) channel for CH_2OO molecules prepared at the S_2^{min} geometry.

We end by reiterating that the richer dynamics predicted here are only relevant when exciting to energies at, or close to, the S_2 minimum. Given the very small cross-section for S_2–S_0 adiabatic excitation, these rival pathways to direct O–O bond fission are expected to make only a very minor contribution to the overall decay of photoexcited gas phase CH_2OO molecules in the troposphere. But similar considerations may be expected to gain in relative importance for larger CIs, and for CIs and other carbonyl oxides in the condensed phase.

Supporting Information

Depictions of the active space orbitals used in the CASSCF/CASPT2 calculations.

Acknowledgements

The work is supported by the National Science Foundation under grant no. 2003422. TNVK also thanks UL Lafayette for start-up funds. Portions of this research were conducted with high performance computational resources provided by the Louisiana Optical Network Infrastructure (http://www.loni.org).

References

(1) Johnson, D.; Marston, G. The Gas-Phase Ozonolysis of Unsaturated Volatile Organic Compounds in the Troposphere. *Chem. Soc. Rev.* **2008**, *37* (4), 699–716. https://doi.org/10.1039/b704260b.

(2) Alam, M. S.; Camredon, M.; Rickard, A. R.; Carr, T.; Wyche, K. P.; Hornsby, K. E.;

Monks, P. S.; Bloss, W. J. Total Radical Yields from Tropospheric Ethene Ozonolysis. *Phys. Chem. Chem. Phys.* **2011**, *13* (23), 11002–11015. https://doi.org/10.1039/c0cp02342f.

(3) Emmerson, K. M.; Carslaw, N. Night-Time Radical Chemistry during the TORCH Campaign. *Atmos. Environ.* **2009**, *43* (20), 3220–3226. https://doi.org/10.1016/j.atmosenv.2009.03.042.

(4) Emmerson, K. M.; Carslaw, N.; Carslaw, D. C.; Lee, J. D.; McFiggans, G.; Bloss, W. J.; Gravestock, T.; Heard, D. E.; Hopkins, J.; Ingham, T.; Pilling, M. J.; Smith, S. C.; Jacob, M.; Monks, P. S. Free Radical Modelling Studies during the UK TORCH Campaign in Summer 2003. *Atmos. Chem. Phys.* **2007**, *7* (1), 167–181. https://doi.org/10.5194/acp-7-167-2007.

(5) Hansen, A. S.; Liu, Z.; Chen, S.; Schumer, M. G.; Walsh, P. J.; Lester, M. I. Unraveling Conformer-Specific Sources of Hydroxyl Radical Production from an Isoprene-Derived Criegee Intermediate by Deuteration. *J. Phys. Chem. A* **2020**, *124* (24), 4929–4938. https://doi.org/10.1021/acs.jpca.0c02867.

(6) Cox, R. A.; Ammann, M.; Crowley, J. N.; Herrmann, H.; Jenkin, M. E.; Faye McNeill, V.; Mellouki, A.; Troe, J.; Wallington, T. J. Evaluated Kinetic and Photochemical Data for Atmospheric Chemistry: Volume VII-Criegee Intermediates. *Atmos. Chem. Phys.* **2020**, *20* (21), 13497–13519. https://doi.org/10.5194/acp-20-13497-2020.

(7) Chhantyal-Pun, R.; Khan, M. A. H.; Taatjes, C. A.; Percival, C. J.; Orr-Ewing, A. J.; Shallcross, D. E. Criegee Intermediates: Production, Detection and Reactivity. *Int. Rev. Phys. Chem.* **2020**, *39* (3), 383–422. https://doi.org/10.1080/0144235X.2020.1792104.

(8) Caravan, R. L.; Vansco, M. F.; Lester, M. I. Open Questions on the Reactivity of Criegee

Intermediates. *Commun. Chem.* **2021**, *4* (1), 44. https://doi.org/10.1038/s42004-021-00483-5.

(9) Mauldin, R. L.; Berndt, T.; Sipilä, M.; Paasonen, P.; Petäjä, T.; Kim, S.; Kurtén, T.; Stratmann, F.; Kerminen, V. M.; Kulmala, M. A New Atmospherically Relevant Oxidant of Sulphur Dioxide. *Nature* **2012**, *488* (7410), 193–196. https://doi.org/10.1038/nature11278.

(10) Stephenson, T. A.; Lester, M. I. Unimolecular Decay Dynamics of Criegee Intermediates: Energy-Resolved Rates, Thermal Rates, and Their Atmospheric Impact. *Int. Rev. Phys. Chem.* **2020**, *39* (1), 1–33. https://doi.org/10.1080/0144235X.2020.1688530.

(11) McGillen, M. R.; Curchod, B. F. E.; Chhantyal-Pun, R.; Beames, J. M.; Watson, N.; Khan, M. A. H.; McMahon, L.; Shallcross, D. E.; Orr-Ewing, A. J. Criegee Intermediate-Alcohol Reactions, A Potential Source of Functionalized Hydroperoxides in the Atmosphere. *ACS Earth Sp. Chem.* **2017**, *1* (10), 664–672. https://doi.org/10.1021/acsearthspacechem.7b00108.

(12) Chhantyal-Pun, R.; Rotavera, B.; McGillen, M. R.; Khan, M. A. H.; Eskola, A. J.; Caravan, R. L.; Blacker, L.; Tew, D. P.; Osborn, D. L.; Percival, C. J.; Taatjes, C. A.; Shallcross, D. E.; Orr-Ewing, A. J. Criegee Intermediate Reactions with Carboxylic Acids: A Potential Source of Secondary Organic Aerosol in the Atmosphere. *ACS Earth Sp. Chem.* **2018**, *2* (8), 833–842. https://doi.org/10.1021/acsearthspacechem.8b00069.

(13) Vereecken, L.; Novelli, A.; Taraborrelli, D. Unimolecular Decay Strongly Limits the Atmospheric Impact of Criegee Intermediates. **2017**, *19* (47), 31599–31612. https://doi.org/10.1039/C7CP05541B.

(14) Bagchi, A.; Yu, Y.; Huang, J. H.; Tsai, C. C.; Hu, W. P.; Wang, C. C. Evidence and

Evolution of Criegee Intermediates, Hydroperoxides and Secondary Organic Aerosols Formed: Via Ozonolysis of α-Pinene. *Phys. Chem. Chem. Phys.* **2020**, *22* (12), 6528–6537. https://doi.org/10.1039/c9cp06306d.

(15) Ting, A. W.-L. L.; Lin, J. J.-M. M. UV Spectrum of the Simplest Deuterated Criegee Intermediate CD2OO. *J. Chinese Chem. Soc.* **2017**, *64* (4), 360–368. https://doi.org/10.1002/jccs.201700049.

(16) Chang, Y. P.; Li, Y. L.; Liu, M. L.; Ou, T. C.; Lin, J. J. M. Absolute Infrared Absorption Cross Section of the Simplest Criegee Intermediate Near 1285.7 Cm-1. *J. Phys. Chem. A* **2018**, *122* (45), 8874–8881. https://doi.org/10.1021/acs.jpca.8b06759.

(17) Foreman, E. S.; Kapnas, K. M.; Jou, Y. T.; Kalinowski, J.; Feng, D.; Gerber, R. B.; Murray, C. High Resolution Absolute Absorption Cross Sections of the B1A′-X1A′ Transition of the CH2OO Biradical. *Phys. Chem. Chem. Phys.* **2015**, *17* (48), 32539–32546. https://doi.org/10.1039/c5cp04977f.

(18) Ting, W. L.; Chen, Y. H.; Chao, W.; Smith, M. C.; Lin, J. J. M. The UV Absorption Spectrum of the Simplest Criegee Intermediate CH 2OO. *Phys. Chem. Chem. Phys.* **2014**, *16* (22), 10438–10443. https://doi.org/10.1039/c4cp00877d.

(19) Smith, M. C.; Ting, W. L.; Chang, C. H.; Takahashi, K.; Boering, K. A.; Lin, J. J. M. UV Absorption Spectrum of the C2 Criegee Intermediate CH3CHOO. *J. Chem. Phys.* **2014**, *141* (7). https://doi.org/10.1063/1.4892582.

(20) Chang, Y.-P. P.; Chang, C.-H. H.; Takahashi, K.; Lin, J. J.-M. M. Absolute UV Absorption Cross Sections of Dimethyl Substituted Criegee Intermediate (CH3)2COO. *Chem. Phys. Lett.* **2016**, *653*, 155–160. https://doi.org/10.1016/j.cplett.2016.04.082.

(21) Sheps, L.; Scully, A. M.; Au, K. UV Absorption Probing of the Conformer-Dependent

Reactivity of a Criegee Intermediate CH3CHOO. *Phys. Chem. Chem. Phys.* **2014**, *16* (48), 26701–26706.

(22) Sheps, L. Absolute Ultraviolet Absorption Spectrum of a Criegee Intermediate CH 2OO. *J. Phys. Chem. Lett.* **2013**, *4* (24), 4201–4205. https://doi.org/10.1021/jz402191w.

(23) Sršeň, Š.; Hollas, D.; Slavíček, P. UV Absorption of Criegee Intermediates: Quantitative Cross Sections from High-Level: Ab Initio Theory. *Phys. Chem. Chem. Phys.* **2018**, *20* (9), 6421–6430. https://doi.org/10.1039/c8cp00199e.

(24) Dawes, R.; Jiang, B.; Guo, H. UV Absorption Spectrum and Photodissociation Channels of the Simplest Criegee Intermediate (CH2OO). *J. Am. Chem. Soc.* **2015**, *137* (1), 50–53. https://doi.org/10.1021/ja510736d.

(25) Aplincourt, P.; Henon, E.; Bohr, F.; Ruiz-López, M. F. Theoretical Study of Photochemical Processes Involving Singlet Excited States of Formaldehyde Carbonyl Oxide in the Atmosphere. *Chem. Phys.* **2002**, *285* (2–3), 221–231. https://doi.org/10.1016/S0301-0104(02)00804-2.

(26) Beames, J. M.; Liu, F.; Lu, L.; Lester, M. I. Ultraviolet Spectrum and Photochemistry of the Simplest Criegee Intermediate CH2OO. *J. Am. Chem. Soc.* **2012**, *134* (49), 20045–20048. https://doi.org/10.1021/ja310603j.

(27) Sheps, L.; Rotavera, B.; Eskola, A. J.; Osborn, D. L.; Taatjes, C. A.; Au, K.; Shallcross, D. E.; Khan, M. A. H.; Percival, C. J. The Reaction of Criegee Intermediate CH2OO with Water Dimer: Primary Products and Atmospheric Impact. *Phys. Chem. Chem. Phys.* **2017**, *19* (33), 21970–21979. https://doi.org/10.1039/c7cp03265j.

(28) Esposito, V. J.; Werba, O.; Bush, S. A.; Marchetti, B.; Karsili, T. N. V. Insights into the Ultrafast Dynamics of CH2OO and CH3CHOO Following Excitation to the Bright 1ππ*

State: The Role of Singlet and Triplet States. *Photochem. Photobiol.* **2021**, *98*, 763–772. https://doi.org/10.1111/php.13560.

(29) McCoy, J. C.; Marchetti, B.; Thodika, M.; Karsili, T. N. V. A Simple and Efficient Method for Simulating the Electronic Absorption Spectra of Criegee Intermediates: Benchmarking on CH2OO and CH3CHOO. *J. Phys. Chem. A* **2021**, *125* (19), 4089–4097. https://doi.org/10.1021/acs.jpca.1c01074.

(30) Esposito, V. J.; Liu, T.; Wang, G.; Caracciolo, A.; Vansco, M. F.; Marchetti, B.; Karsili, T. N. V.; Lester, M. I. Photodissociation Dynamics of CH2OO on Multiple Potential Energy Surfaces: Experiment and Theory. *J. Phys. Chem. A* **2021**, *125* (30), 6571–6579. https://doi.org/10.1021/acs.jpca.1c03643.

(31) Vansco, M. F.; Marchetti, B.; Lester, M. I. Electronic Spectroscopy of Methyl Vinyl Ketone Oxide: A Four-Carbon Unsaturated Criegee Intermediate from Isoprene Ozonolysis. *J. Chem. Phys.* **2018**, *149* (24), 244309. https://doi.org/10.1063/1.5064716.

(32) Vansco, M. F.; Marchetti, B.; Trongsiriwat, N.; Bhagde, T.; Wang, G.; Walsh, P. J.; Klippenstein, S. J.; Lester, M. I. Synthesis, Electronic Spectroscopy, and Photochemistry of Methacrolein Oxide: A Four-Carbon Unsaturated Criegee Intermediate from Isoprene Ozonolysis. *J. Am. Chem. Soc.* **2019**, *141* (38), 15058–15069. https://doi.org/10.1021/jacs.9b05193.

(33) Wang, G.; Liu, T.; Caracciolo, A.; Vansco, M. F.; Trongsiriwat, N.; Walsh, P. J.; Marchetti, B.; Karsili, T. N. V; Lester, M. I. Photodissociation Dynamics of Methyl Vinyl Ketone Oxide: A Four-Carbon Unsaturated Criegee Intermediate from Isoprene Ozonolysis. *J. Chem. Phys.* **2021**, *155* (17), 174305. https://doi.org/10.1063/5.0068664.

(34) Lin, Y. H.; Takahashi, K.; Lin, J. J. M. Absolute Photodissociation Cross Sections of

Thermalized Methyl Vinyl Ketone Oxide and Methacrolein Oxide. *Phys. Chem. Chem. Phys.* **2022**, *24* (17), 10439–10450. https://doi.org/10.1039/d2cp00476c.

(35) Lin, Y. H.; Yin, C.; Takahashi, K.; Lin, J. J. M. Surprisingly Long Lifetime of Methacrolein Oxide, an Isoprene Derived Criegee Intermediate, under Humid Conditions. *Commun. Chem.* **2021**, *4* (1), 1–20. https://doi.org/10.1038/s42004-021-00451-z.

(36) Vansco, M. F.; Zuraski, K.; Winiberg, F. A. F.; Au, K.; Trongsiriwat, N.; Walsh, P. J.; Osborn, D. L.; Percival, C. J.; Klippenstein, S. J.; Taatjes, C. A.; Lester, M. I.; Caravan, R. L. Functionalized Hydroperoxide Formation from the Reaction of Methacrolein-oxide, an Isoprene-derived Criegee Intermediate, with Formic Acid: Experiment and Theory. *Molecules* **2021**, *26* (10), 3058. https://doi.org/10.3390/molecules26103058.

(37) Caravan, R. L.; Vansco, M. F.; Au, K.; Khan, A. A. H.; Li, Y.-L. L.; Winiberg, F. A. F. F.; Zuraski, K.; Lin, Y.-H. H.; Chao, W.; Trongsiriwat, N.; Walsh, P. J.; Osborn, D. L.; Percival, C. J.; Lin, J. J.-M. M.; Shallcross, D. E.; Sheps, L.; Klippenstein, S. J.; Taatjes, C. A.; Lester, M. I.; Khan, M. A. H.; Li, Y.-L. L.; Winiberg, F. A. F. F.; Zuraski, K.; Lin, Y.-H. H.; Chao, W.; Trongsiriwat, N.; Walsh, P. J.; Osborn, D. L.; Percival, C. J.; Lin, J. J.-M. M.; Shallcross, D. E.; Sheps, L.; Klippenstein, S. J.; Taatjes, C. A.; Lester, M. I. Direct Kinetic Measurements and Theoretical Predictions of an Isoprene-Derived Criegee Intermediate. *Proc. Natl. Acad. Sci.* **2020**, *117* (18), 9733 LP – 9740. https://doi.org/10.1073/pnas.1916711117.

(38) Nguyen, T. B.; Tyndall, G. S.; Crounse, J. D.; Teng, A. P.; Bates, K. H.; Schwantes, R. H.; Coggon, M. M.; Zhang, L.; Feiner, P.; Milller, D. O.; Skog, K. M.; Rivera-Rios, J. C.; Dorris, M.; Olson, K. F.; Koss, A.; Wild, R. J.; Brown, S. S.; Goldstein, A. H.; De Gouw, J. A.; Brune, W. H.; Keutsch, F. N.; Seinfeld, J. H.; Wennberg, P. O. Atmospheric Fates

of Criegee Intermediates in the Ozonolysis of Isoprene. *Phys. Chem. Chem. Phys.* **2016**, *18* (15), 10241–10254. https://doi.org/10.1039/c6cp00053c.

(39) Sindelarova, K.; Granier, C.; Bouarar, I.; Guenther, A.; Tilmes, S.; Stavrakou, T.; Müller, J. F.; Kuhn, U.; Stefani, P.; Knorr, W. Global Data Set of Biogenic VOC Emissions Calculated by the MEGAN Model over the Last 30 Years. *Atmos. Chem. Phys.* **2014**, *14* (17), 9317–9341. https://doi.org/10.5194/acp-14-9317-2014.

(40) Nikoobakht, B.; Köppel, H. UV Absorption Spectrum and Photodissociation Dynamics of CH2OO Following Excitation to the B1 A′ State. *Mol. Phys.* **2021**, *119* (21–22), e1958019. https://doi.org/10.1080/00268976.2021.1958019.

(41) Nikoobakht, B.; Köppel, H. Correlated Quantum Treatment of the Photodissociation Dynamics of Formaldehyde Oxide CH2OO. *Phys. Chem. Chem. Phys.* **2022**, *24* (20), 12433–12441. https://doi.org/10.1039/D2CP01007K.

(42) Antwi, E.; Bush, R.; Marchetti, B.; Karsili, T. A Direct Dynamics Study of the Exotic Photochemistry of the Simplest Criegee Intermediate, CH2OO. *Phys. Chem. Chem. Phys.* **2022**, *24*, 16724–16731. https://doi.org/10.1039/d2cp01860h.

(43) Li, Y.; Gong, Q.; Yue, L.; Wang, W.; Liu, F. Photochemistry of the Simplest Criegee Intermediate, CH2OO: Photoisomerization Channel toward Dioxirane Revealed by CASPT2 Calculations and Trajectory Surface-Hopping Dynamics. *J. Phys. Chem. Lett.* **2018**, *9* (5), 978–981. https://doi.org/10.1021/acs.jpclett.8b00023.

(44) Frisch, M. J.; Trucks, G. W.; Schlegel, H. B.; Scuseria, G. E.; Robb, M. A.; Cheeseman, J. R.; Scalmani, G.; Barone, V.; Mennucci, B.; Petersson, G. A.; Nakatsuji, H.; Caricato, M.; Li, X.; Hratchian, H. P.; Izmaylov, A. F.; Bloino, J.; Zheng, G.; Sonnenberg, J. L.; Hada, M.; Ehara, M.; Toyota, K.; Fukuda, R.; Hasegawa, J.; Ishida, M.; Nakajima, T.; Honda,

Y.; Kitao, O.; Nakai, H.; Vreven, T.; Montgomery Jr., J. A.; Peralta, J. E.; Ogliaro, F.; Bearpark, M.; Heyd, J. J.; Brothers, E.; Kudin, K. N.; Staroverov, V. N.; Kobayashi, R.; Normand, J.; Raghavachari, K.; Rendell, A.; Burant, J. C.; Iyengar, S. S.; Tomasi, J.; Cossi, M.; Rega, N.; Millam, N. J.; Klene, M.; Knox, J. E.; Cross, J. B.; Bakken, V.; Adamo, C.; Jaramillo, J.; Gomperts, R.; Stratmann, R. E.; Yazyev, O.; Austin, A. J.; Cammi, R.; Pomelli, C.; Ochterski, J. W.; Martin, R. L.; Morokuma, K.; Zakrzewski, V. G.; Voth, G. A.; Salvador, P.; Dannenberg, J. J.; Dapprich, S.; Daniels, A. D.; Farkas, Ö.; Foresman, J. B.; Ortiz, J. V; Cioslowski, J.; Fox, D. J. Gaussian 16, Revision C.01. *Gaussian Inc. Wallingford CT* **2016**.

(45) Lee, E. P. F.; Mok, D. K. W.; Shallcross, D. E.; Percival, C. J.; Osborn, D. L.; Taatjes, C. A.; Dyke, J. M. Spectroscopy of the Simplest Criegee Intermediate CH 2OO: Simulation of the First Bands in Its Electronic and Photoelectron Spectra. *Chem. - A Eur. J.* **2012**, *18* (39), 12411–12423. https://doi.org/10.1002/chem.201200848.

(46) Barbatti, M.; Granucci, G.; Persico, M.; Ruckenbauer, M.; Vazdar, M.; Eckert-Maksić, M.; Lischka, H. The On-the-Fly Surface-Hopping Program System Newton-X: Application to Ab Initio Simulation of the Nonadiabatic Photodynamics of Benchmark Systems. *J. Photochem. Photobiol. A Chem.* **2007**, *190* (2–3), 228–240. https://doi.org/10.1016/j.jphotochem.2006.12.008.

(47) Barbatti, M.; Ruckenbauer, M.; Plasser, F.; Pittner, J.; Granucci, G.; Persico, M.; Lischka, H. Newton-X: A Surface-Hopping Program for Nonadiabatic Molecular Dynamics. *Wiley Interdiscip. Rev. Comput. Mol. Sci.* **2014**, *4* (1), 26–33. https://doi.org/10.1002/wcms.1158.

(48) Butcher, J. C. A Modified Multistep Method for the Numerical Integration of Ordinary

Differential Equations. *J. ACM* **1965**, *12* (1), 124–135. https://doi.org/10.1145/321250.321261.

(49) Park, J. W.; Shiozaki, T. Analytical Derivative Coupling for Multistate CASPT2 Theory. *J. Chem. Theory Comput.* **2017**, *13* (6), 2561–2570. https://doi.org/10.1021/acs.jctc.7b00018.

(50) Antwi, E.; Bush, R.; Marchetti, B.; Karsili, T. Climbing up Conical Intersections: A Direct Dynamics Study of the Exotic Photochemistry of Criegee Intermediates. *Phys. Chem. Chem. Phys.* **2022**. https://doi.org/10.1039/D2CP01860H.

(51) Shiozaki, T. BAGEL: Brilliantly Advanced General Electronic-Structure Library. *Wiley Interdiscip. Rev. Comput. Mol. Sci.* **2018**, *8* (1), e1331. https://doi.org/10.1002/wcms.1331.

(52) Werner, H. J.; Knowles, P. J.; Knizia, G.; Manby, F. R.; Schütz, M. Molpro: A General-Purpose Quantum Chemistry Program Package. *Wiley Interdiscip. Rev. Comput. Mol. Sci.* **2012**, *2* (2), 242–253. https://doi.org/10.1002/wcms.82.

(53) Werner, H.-J.; Knowles, P. J.; Knizia, G.; Manby, F. R.; Schütz, M.; Celani, P.; Györffy, W.; Kats, D.; Korona, T.; Lindh, R.; Mitrushenkov, A.; Rauhut, G.; Shamasundar, K. R.; Adler, T. B.; Amos, R. D.; Bennie, S.; Bernhardsson, A.; Berning, A.; Cooper, D. L.; Deegan, M. J. O.; Dobbyn, A. J.; Eckert, F.; Goll, E.; Hampel, C.; Hesselmann, A.; Hetzer, G.; Hrenar, T.; Jansen, G.; Köppl, C.; Lee, S. J. R.; Liu, Y.; Lloyd, A. W.; Ma, Q.; Mata, R. A.; May, A. J.; McNicholas, S. J.; Meyer, W.; III, T. F. M.; Mura, M. E.; Nicklass, A.; O'Neill, D. P.; Palmieri, P.; Peng, D.; Pflüger, K.; Pitzer, R.; Reiher, M.; Shiozaki, T.; Stoll, H.; Stone, A. J.; Tarroni, R.; Thorsteinsson, T.; Wang, M.; Welborn, M. MOLPRO, Version 2018.1, a Package of Ab Initio Programs. **2018**.

(54) Nakajima, M.; Endo, Y. Communication: Determination of the Molecular Structure of the Simplest Criegee Intermediate CH2OO. *J. Chem. Phys.* **2013**, *139* (10), 101103. https://doi.org/10.1063/1.4821165.

(55) Karsili, T. N. V; Marchetti, B.; Lester, M. I.; Ashfold, M. N. R. Electronic Absorption Spectroscopy and Photochemistry of Criegee Intermediates. *Photochem. Photobiol.* **2022**, https://doi.org/https://doi.org/10.1111/php.13665.

(56) Beames, J. M.; Liu, F.; Lu, L.; Lester, M. I. UV Spectroscopic Characterization of an Alkyl Substituted Criegee Intermediate CH3CHOO. *J. Chem. Phys.* **2013**, *138* (24), 244307. https://doi.org/10.1063/1.4810865.

Table of Contents Graphic